A Fully-Integrated Penta-Band Tx Reconfigurable Power Amplifier with SOI CMOS Switches for Mobile Handset Applications

Unha Kim, Sungyoon Kang, Junghyun Kim, and Youngwoo Kwon

A fully-integrated penta-band reconfigurable power amplifier (PA) is developed for handset Tx applications. The output structure of the proposed PA is composed of the fixed output matching network, power and frequency reconfigurable networks, and post-PA distribution switches. In this work, a new reconfiguration technique is proposed for a specific band requiring power and frequency reconfiguration simultaneously. The design parameters for the proposed reconfiguration are newly derived and applied to the PA. To reduce the module size, the switches of reconfigurable output networks and post-PA switches are integrated into a single IC using a 0.18 μm silicon-on-insulator CMOS process, and a compact size of 5 mm × 5 mm is thus achieved. The fabricated W-CDMA PA module shows adjacent channel leakage ratios better than –39 dBc up to the rated linear power and power-added efficiencies of higher than around 38% at the maximum linear output power over all the bands. Efficiency degradation is limited to 2.5% to 3% compared to the single-band reference PA.

Keywords: Band switching, multi-band, power amplifier, PA, reconfigurable, silicon-on-insulator, SOI, W-CDMA.

Manuscript received August 31, 2013; revised October 17, 2013; accepted Nov. 5, 2013.

This work was supported by the National Research Foundation of Korea (NRF) grant funded by the Korea Government (MSIP) (No. 2013R1A1A2013345, No. 2013R1A2A1A05006502).

Unha Kim (phone: +82 2 880 8461, edmaun1@snu.ac.kr) and Youngwoo Kwon (ykwon@snu.ac.kr) are with the School of Electrical Engineering and Computer Science and INMC, Seoul National University, Seoul, Rep. of Korea.

Sungyoon Kang (kksy@hanyang.ac.kr) and Junghyun Kim (corresponding author, junhkim@hanyang.ac.kr) are with the Department of Electronics and System Engineering, Hanyang University, Ansan, Rep. of Korea.

I. Introduction

For the last decade, multi-band power amplifiers (PAs) have become a key component for the Tx front end of mobile handsets, which enables worldwide global roaming service and extends data transmission capacity. To cover the ever-increasing number of 3G UMTS frequency bands, PA manufacturers have used the conventional multi-band PA design approach, wherein a dedicated single-band PA is added for each additional frequency band [1] while putting up with increases in module sizes and development costs. Recently, works to implement multi-band PAs with a single PA core were developed to reduce the module size and save on cost. There are two approaches to implementing a PA for these purposes: broadband matching technique [2]-[4] and reconfigurable matching technique [5]-[9].

The broadband matching technique (shown in Fig. 1(a)) was recently adopted for commercial use by PA manufacturers because it can simply implement a PA using a single output matching block. However, bulky post-PA switch blocks should be added to provide multiple paths for multi-band PA implementation. Additionally, the number of broadband matching sections should be increased as the fractional bandwidth is increased, thus resulting in higher loss and size increase [2], [3]. In addition, if the target output powers are different among the covered frequency bands, this technique cannot guarantee maximized efficiency at some bands, meaning that additional matching (causing circuit complexity) could be needed at each output. A pseudomorphic high-electron-mobility transistor (pHEMT) broadband multi-band

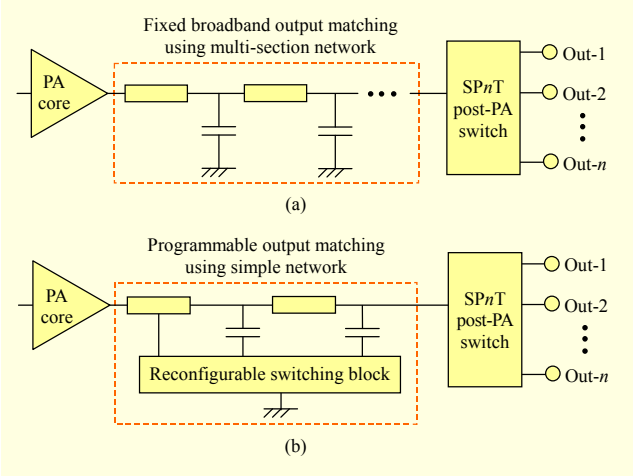

Fig. 1. Conceptual schematic of multi-band (a) broadband PA and (b) reconfigurable PA.

PA was recently reported showing desirable performance, but it would not be useful for commercial use due to its bulky die and module size [4].

The reconfigurable matching technique is depicted in Fig. 1(b). The programmable output matching network (OMN) of the reconfigurable PA provides optimum matching with simple switch blocks for each band while minimizing RF performance degradation [5]-[9]. A new approach for multi-band reconfigurable PAs for practical handset applications was recently introduced in our previous work [8], wherein the frequency bands were grouped into high-band and low-band to avoid complication and performance degradation in covering a frequency range that was too wide. With discrete PIN diode switch blocks, a "frequency" reconfigurable OMN was used for band-5 implementation in the band-8 (natural frequency band in low-band) path, and a "power" reconfigurable OMN was used for band-4 implementation in the band-2 (natural frequency band in high-band) path, covering five popular UMTS frequency bands with a dedicated band-1 path. However, it is worthwhile to note that in [8], it is not easy to optimize band-4 performance with just a power reconfigurable OMN due to the frequency difference (11%) between band-2 and band-4, which means that a new investigation into how best to reconfigure power and frequency simultaneously is required in order to optimize band-4 performance. In addition, even though discrete micro-electro-mechanical systems (MEMS) and semiconductor switches used in [6]-[9] showed desirable performance, they are still difficult to adopt for practical PA application due to such issues as actuation voltage, reliability, and particularly, integration capability for PA size reduction and cost saving. Besides, two additional SP2T switches must be used externally at the PA outputs in [8] if five popular frequency bands are all requested with one PA module.

In this work, a fully integrated penta-band reconfigurable PA is implemented for UMTS handset applications. Since the silicon-on-insulator (SOI) CMOS can be a good candidate thanks to its smaller parasitic capacitance and high power-handling capability over bulk CMOS [10]-[13], all the switch blocks for reconfigurable OMNs are integrated in a single SOI CMOS IC, and the PA logic controller and most of the passive elements of the reconfigurable OMNs are integrated into the IC as well. Additional post-PA switches for penta-band PA operation are also integrated into the single SOI CMOS IC, facilitating the implementation of a penta-band PA with five outputs, which allows the PA to be implemented with a smaller module size and lower cost. Furthermore, an extended reconfigurable OMN that reconfigures frequency and power simultaneously with a single matching network is proposed and the expectation is that performance will be optimized for the specific band that is reconfigured from the natural band for both frequency and linear output power.

Detailed design analysis and parameters of the newly proposed reconfiguration are quantitatively introduced in section II, followed by the circuit description, also in section III. The measurement results and conclusion are presented in sections IV and V, respectively.

II. PA Overview and Design Parameter Derivation of Power and Frequency Reconfigurable Network

The block diagram and the target spec of the proposed reconfigurable PA are shown in Fig. 2 and Table 1, respectively. This PA has five outputs to fulfill penta-band UMTS operation using the post-PA distribution switches. To mitigate the complication in covering too wide a frequency range, the PA is categorized as either a low-band (0.8 GHz to 0.9 GHz) PA or a high-band (1.7 GHz to 2.0 GHz) PA. Each PA has a fixed output matching network (FOMN), which is optimized for the natural frequency band (f_N) when the PA is not reconfigured. When the PA is reconfigured, the power and/or frequency reconfigurable network is thus operated in conjunction with the

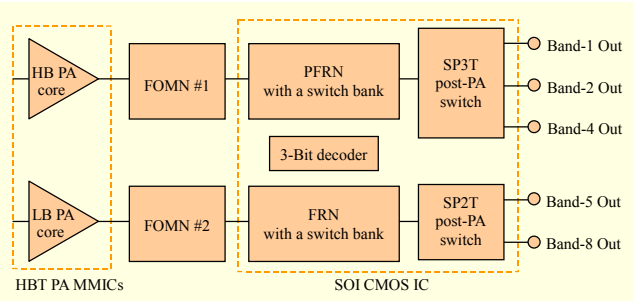

Fig. 2. Block diagram of the proposed penta-band UMTS reconfigurable PA.

Table 1. UMTS frequencies and target linear output powers.

Band	Tx frequency (MHz)	Rx frequency (MHz)	Target P_{out} (dBm)
Band-1	1,920 - 1,980	2,110 - 2,170	28.0
Band-2	1,850 - 1,910	1,930 - 1,990	28.5
Band-4	1,710 - 1,755	2,110 - 2,155	27.5
Band-5	824 - 849	869 - 894	28.2
Band-8	880 - 915	925 - 960	28.2

FOMN and the PA is optimized for the reconfigured frequency (f_R) with either the same or different target output power. In this work, band-2 (band-8) is the natural band and band-4 (band-5) is the reconfigured band for high-band (low-band) operation. Since the difference between band-2 and band-1, in terms of the target output power and frequency, is small, no reconfiguration is performed for band-1 operation. For band-5 reconfiguration, the frequency reconfigurable network (FRN), which was already covered in [8], is used since little power difference exists between the two bands.

The primary goal of this section is to obtain closed-form formulae for the optimum design parameters of the proposed reconfigurable matching network (for the specific band requiring power reconfiguration and frequency reconfiguration simultaneously.) Contrary to the band-1 case, when band-4 is reconfigured from the natural band (band-2 in this work), both the frequency difference (11%) and power difference (1 dB) between band-2 and band-4 cannot be neglected, and band-4 thus should be reconfigured with both power and frequency simultaneously. It means that the analysis of the power reconfigurable network (PRN) in our previous work [8], should be extended to the power and frequency reconfigurable network (PFRN) for band-4 in this work, so as to obtain optimum performance.

Quantitative analysis can be achieved by adding the frequency scaling factor ($\beta = f_R / f_N$) in the PRN, as shown in Fig. 3. The PFRN consists of a shunt inductive element (L_R) and a series transmission line (θ_R), which are the design parameters for the reconfiguration. When the shunt switch is off (as is state), FOMN provides the optimum load impedance ($Z_L = R_{opt}$) at the natural frequency band (f_N). If the output network is reconfigured (switch on), the load impedance is increased according to the backed-off power. As a power back-off of P_{BO} dB is required, the load impedance (Z_L) should be changed to $M \times R_{opt}$, where $M = 10^{P_{BO}/10}$. Using the principle that the impedance trajectory of PFRN moves along the constant g-circle and constant Γ-circle, a quadratic equation on θ_R at f_R ($\theta'_R = \beta\theta_R$) is derived as

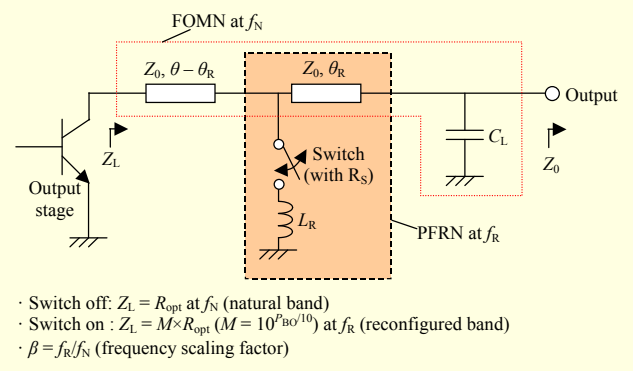

Fig. 3. Schematic of PFRN.

Table 2. Available reconfiguration condition of PFRN.

Condition*		Reconfigured band (compared to natural band)	Reconfigurability
$P_{BO} < 0$		Higher P_{out}	No
$P_{BO} > 0$	$\beta = 1$	Smaller P_{out}, same frequency	Available
	$\beta < 1$	Smaller P_{out}, lower frequency	Partially available
	$\beta > 1$	Smaller P_{out}, higher frequency	

* Unit of power back-off (P_{BO}) is dB.

$$a \tan^2 \theta'_R + b \tan \theta'_R + c = 0, \quad (1)$$

$$a = X(K^2 + 1) - (MR_{opt} \tan \theta')^2 - Z_0^2, \quad (2)$$

$$b = -2XK - 2(MR_{opt})^2 \tan \theta' + 2Z_0^2 \tan \theta', \quad (3)$$

$$c = X - (MR_{opt})^2 + (Z_0 \tan \theta')^2, \quad (4)$$

where

$$X = Z_0 MR_{opt}(1 + \tan^2 \theta'), \quad (5)$$

$$K = \beta(Z_0 - R_{opt}) \Big/ \sqrt{Z_0 R_{opt}}, \quad (6)$$

and

$$\theta' = \beta\theta = \beta \tan^{-1}\left(\sqrt{R_{opt}/Z_0}\right). \quad (7)$$

To have a solution in (1), $b^2 - 4ac \geq 0$ and $0 \leq \theta'_R \leq \theta'$ should be met as a prerequisite. With the conditions, the analysis shows that one cannot have any solution (θ_R) for $P_{BO} < 0$, which means that the proposed PFRN is available in the case of the reconfigured band requiring a backed-off linear power from the natural band ($P_{BO} > 0$). From the results of (1) through (7), the available reconfiguration conditions of the PFRN are summarized in Table 2. It is worthwhile to note, that in Table 2 the minimum available power back-off ($P_{BO.MIN}$) level exists according to the condition of β. When $\beta = 1$, $P_{BO.MIN}$ is zero,

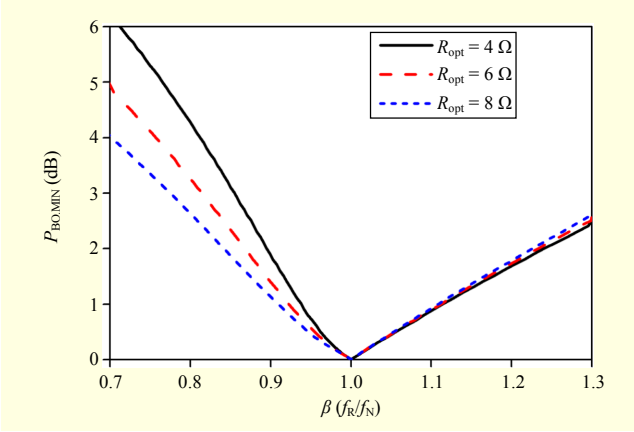

Fig. 4. Minimum available power back-off ($P_{BO.MIN}$) of PFRN as a function of frequency scaling factor (β) for various R_{opt}'s.

and an optimum matching value (θ_R) always exists as a solution corresponding to the target power back-off (P_{BO}). When $\beta \neq 1$, however, the solution of θ_R is limited, and an optimum matching is thus available only in the case of the target $P_{BO} \geq P_{BO.MIN}$. In Fig. 4, $P_{BO.MIN}$ for having a solution of θ_R is plotted as a function of β. It should be noted in Fig. 4 that $P_{BO.MIN}$ depends on R_{opt} as well as β. As R_{opt} increases, $P_{BO.MIN}$ decreases for $\beta < 1$. Once θ_R from (1) is obtained using the well-known Quadratic formula, L_R can simply be calculated from typical circuit theory as

$$L_R = 1/\omega_R (B_2 - B_1), \tag{8}$$

where

$$B_1 = \frac{1}{Z_0} \frac{\tan(\theta' - \theta'_R)\{Z_0^2 - (MR_{opt})^2\}}{(MR_{opt})^2 + \{Z_0 \tan(\theta' - \theta'_R)\}^2} \tag{9}$$

and

$$B_2 = \frac{1}{Z_0} \frac{K(1 - K\tan\theta'_R - \tan^2\theta'_R)}{(1 - K\tan\theta'_R)^2 + \tan^2\theta'_R}. \tag{10}$$

Figure 5 shows the calculated θ_R and $\omega_R L_R$ as a function of β for various P_{BO}'s. From the above result, it is clear that θ_R and $\omega_R L_R$ achieve reconfiguration from the natural band (band-2) to the reconfigurable band (band-4, $R_{opt,B2} = 4.5\ \Omega$, $P_{BO} = 1$ dB, $\beta = 0.92$), which leads to improved performance in band-4.

For the PFRN calculation, the switch in Fig. 3 is assumed to be lossless ($R_S = 0$). When the switch is not completely lossless, the effect of R_S on the PA performance can be represented as the reconfiguration loss. Figure 6 shows the calculated reconfiguration loss of the PFRN as functions of P_{BO} and β for $R_{opt} = 5\ \Omega$ and $R_S = 1\ \Omega$. It is noteworthy that the reconfiguration loss is a strong function of R_S, especially when P_{BO} and β are large. However, the R_S effect can be reduced when its value is smaller than $\omega_R L_R$.

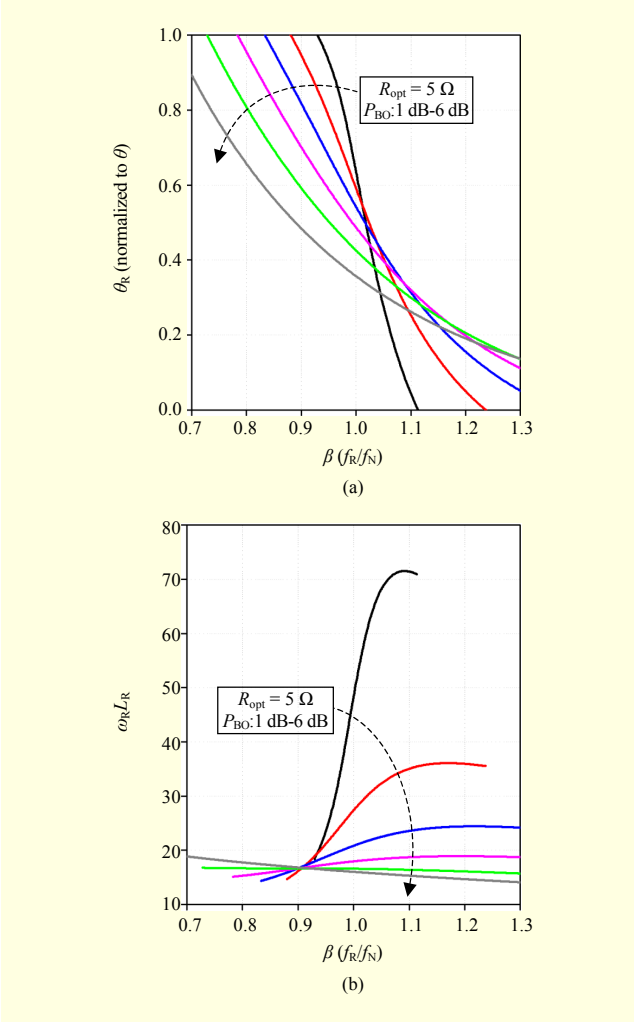

Fig. 5. Required electrical line length and inductive reactance of PFRN as a function of frequency scaling factor (β) for various P_{BO}'s with $R_{opt} = 5\ \Omega$: (a) θ_R at f_R (normalized to θ at f_N) and (b) $\omega_R L_R$.

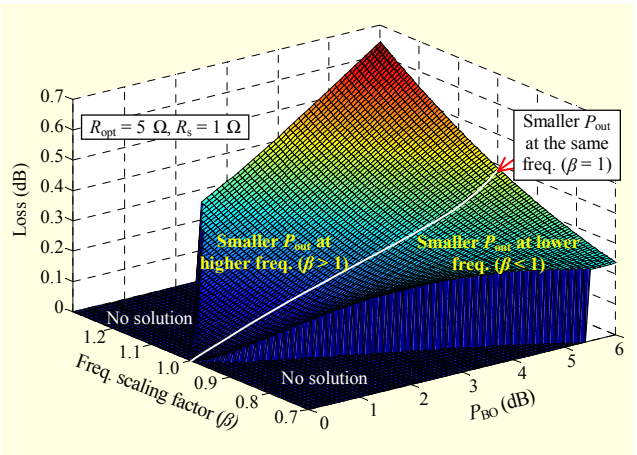

Fig. 6. Reconfiguration loss of PFRN as functions of power back-off (P_{BO}) and frequency scaling factor (β) for R_{opt} = 5 Ω and R_S = 1 Ω.

III. Penta-Band UMTS Reconfigurable PA Design

1. Circuit Description

A fully integrated 5 mm × 5 mm penta-band reconfigurable PA module is designed and fabricated to verify the proposed reconfiguration idea. Figure 7 shows the schematic of the reconfigurable PA. The PA has two inputs and five reconfigurable outputs for popular 5-band UMTS applications. The PA module contains two reconfigurable OMNs and two integrated three-stage PA monolithic microwave integrated circuits (MMICs) for high-and low-frequency UMTS bands, respectively. In the case of high-band PA, the natural band and reconfigured band are band-2 and band-4, respectively. Also, in the case of the low-band PA, the natural band and reconfigured band are band-8 and band-5, respectively where band-1 is dedicated to sharing the same high-band network. Based on the design parameters of the PFRN derived in section II, the performance of band-4 reconfiguration is optimized. For band-5 reconfiguration, the design parameters of the FRN described in [8] are used.

The reconfigurable OMNs are implemented using the lumped elements and transmission lines on a 370 μm thick, seven-layer substrate ($\varepsilon_r \approx 4.7$, $\tan\delta = 0.02$). In Fig. 7, C_1 and C_2 are the surface-mount type capacitors of FOMNs optimized for the natural bands, whereas L_R and C_f are the reconfigurable elements for PFRN and FRN, respectively. Three capacitors, C_{B1} to C_{B3}, are used for DC blocking and C_{B4} as the bypass capacitor. Two bias lines, l_{B1} and l_{B2}, are implemented on inner layers of the substrate.

The PA MMICs are designed and fabricated using a 2 μm InGaP/GaAs HBT process. They are based on a three-stage amplifier design, and the emitter area of the pre-stage (Q1 and Q4), driver stage (Q2 and Q5), main stage for the high-band (Q3), and main stage for the low-band (Q6) are designed to be 240 μm^2, 1,440 μm^2, 5,760 μm^2, and 6,768 μm^2, respectively. The low-pass type input matching networks and high-pass type interstage matching networks were integrated in the MMICs. Two shunt capacitors, C_{m1} and C_{m2}, were added at the collectors of Q3 and Q6, respectively, for harmonic termination. To enhance the efficiency in the low-output-power region, in which UMTS PAs are operated most of the time, the PAs are designed to bypass main stages below 16 dBm [14]. The shunt arm of switch (M_5) and the wire-bond inductor (l_{L1}) assist the PA in reaching optimum performance during low-power-mode operation. The die size of each PA MMIC is 1.1 mm × 1.08 mm.

2. Switch Design Consideration

In Fig. 7, most switches are used for output reconfigurations. This means that the switches must provide low loss and high power capability since the efficiency degradation resulting from the output loss cannot be recovered and the output RF voltage swing is very large. Because the reconfiguration losses are affected by switch R_S, SOI switches are designed to have small R_S and high power capability by increasing the gate width of, and by the stacking of, field-effect transistors (FETs).

The SOI CMOS process used in this work offers 2.5 V *n*MOS FETs with gate oxide thickness of 52 Å and gate length

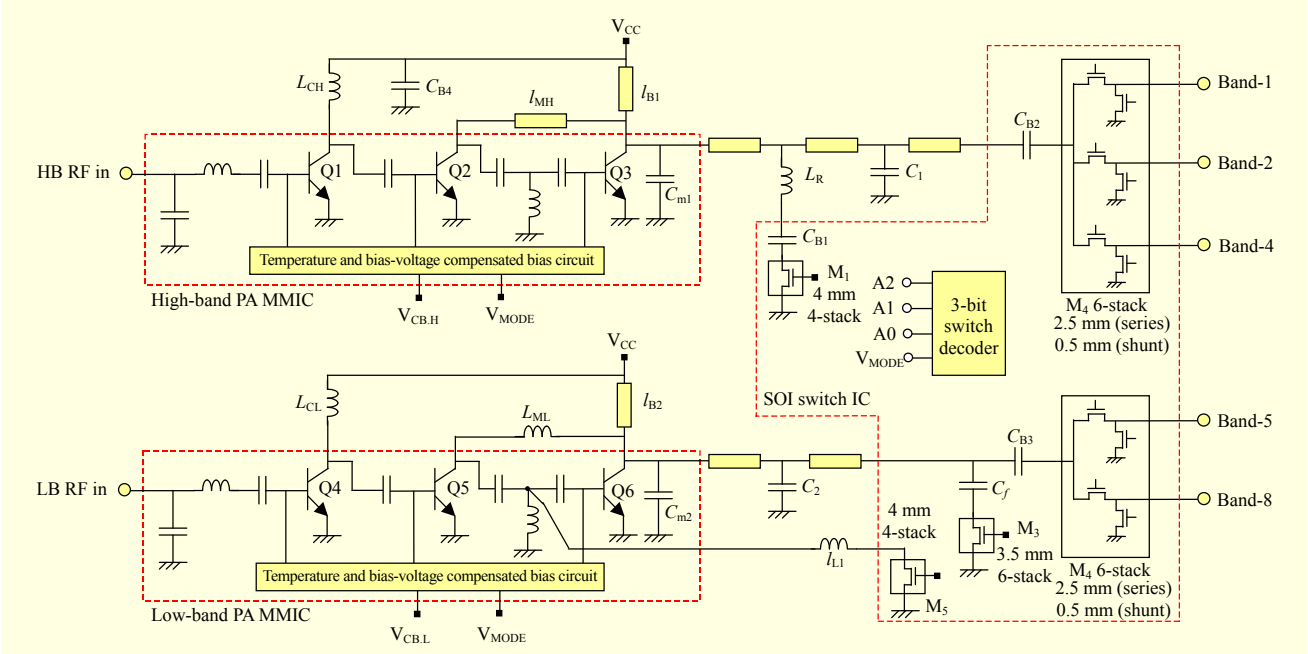

Fig. 7. Schematic of proposed reconfigurable PA module.

ETRI Journal, Volume 36, Number 2, April 2014
http://dx.doi.org/10.4218/etrij.14.2113.0046

Table 3. Switch technologies and their characteristics.

Characteristics	SOI	PIN diode [8]	pHEMT [12]
R_S (Ω)	0.8 Ω·mm	1.0	1.9
C_{off} (fF)	310 fF/mm	400	147
FOM (R_S·C_{off}) (fsec)	250	400	280
Power endurance (dBm)	20log(N×V_m)+10	> 38	> 35

N: number of stacks

V_m: rated drain-source voltage of single NFET (approx. 3.3 V)

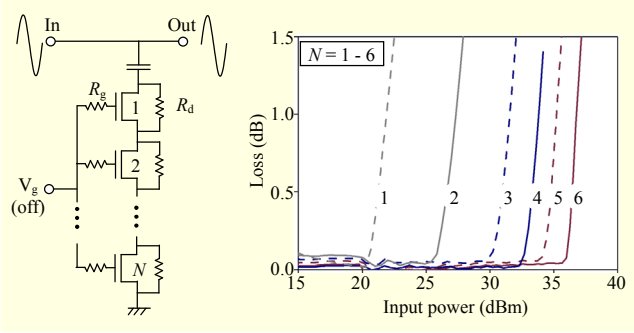

Fig. 8. Measured power endurance of SOI switch for various numbers of stacks (N).

of 0.32 μm. A single NFET provides an R_S of 0.8 Ω·mm and parasitic capacitance (C_{off}) of 310 fF/mm, resulting in an R_S·C_{off} constant (figure of merit (FOM)) of 250 fsec. Typical characteristics of the commercial switches are summarized in Table 3. Compared to the PIN diode and pHEMT switches, the SOI switch offers favorable FOM and its power capability can easily be extended by stacking. SOI switches, each with a different number of stacks (N), are tested to experimentally validate the power handling. Figure 8 shows the measured power endurance of an N-stacked switch, from which one can see that V_m in Table 3 is approximately 3.3 V. To evenly distribute RF voltage to each FET, the gate resistance (R_g in Fig. 8) should be large enough [10]. The switch type of this work is floating-body, which shows slightly better insertion loss and less complexity than the body-contact type. Even if the harmonic distortion characteristic of the floating-body type switch is worse than the body-contact type switch, it can be neglected when switches are used in the reconfigurable OMN and post-PA switch, since most of the harmonic distortions are generated from the PA core [13].

It should be noted that the R_S effect on loss of PFRN is usually larger than that of FRN. In addition, voltage swing is greater at the node in which the forward impedance is higher, even if the delivered power is identical. Based on these considerations, the switches for PFRN and for FRN, M_1 and M_3 in Fig. 7, are designed to primarily have smaller R_S and higher power handling, respectively. It should also be noted that too wide a gate width for R_S reduction leads to excessive C_{off}, resulting in performance degradation by mismatch at the switch-off state. The SP2T and SP3T switches (M_3 and M_2) are designed to have an insertion loss of 0.2 dB to 0.25 dB and an isolation of more than 30 dB, whilst still maintaining a power capability of more than 35 dBm. The fabricated SOI switch IC occupies a die area of 1.0 mm × 1.25 mm.

IV. Measurement Results

The fabricated ICs and PA module are shown in Figs. 9 and 10. The PA module works with a 3.5 V supply, and the 3GPP uplink W-CDMA signal (Rel'99) is used for the PA measurement. The operating voltage of the SOI switch is 2.5 V for "on" and –2 V for "off." Prior to the W-CDMA test, the post-PA switches (M_2 and M_4 in Fig. 7) are measured on-wafer. Figure 11 shows the measured loss, isolation, and power endurance of the SP2T and SP3T switches. Since the switches have parasitic capacitances, the mismatch effect is corrected and net loss (maximum available gain (MAG)) is thus plotted instead of insertion loss. In the case of the SP2T (SP3T) switch at the low-band (high-band) frequency, a loss of 0.2 dB (0.25 dB) and isolation of better than 33 dB (28.5 dB) are measured. The measured power endurance ($P_{0.1dB}$) is 35.8 dBm,

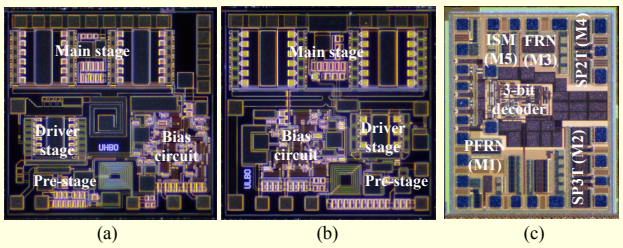

Fig. 9. Chip photographs: (a) high-band PA MMIC, (b) low-band PA MMIC, and (c) SOI CMOS switch IC.

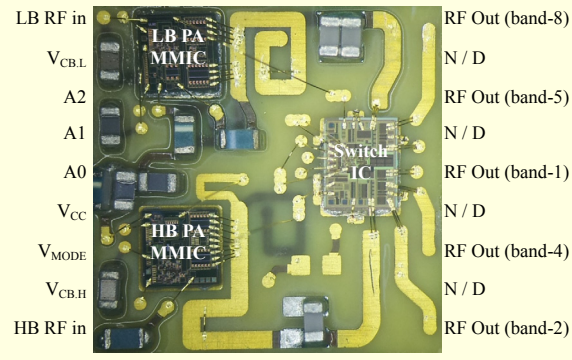

Fig. 10. Photograph of fabricated 5 mm × 5 mm PA module.

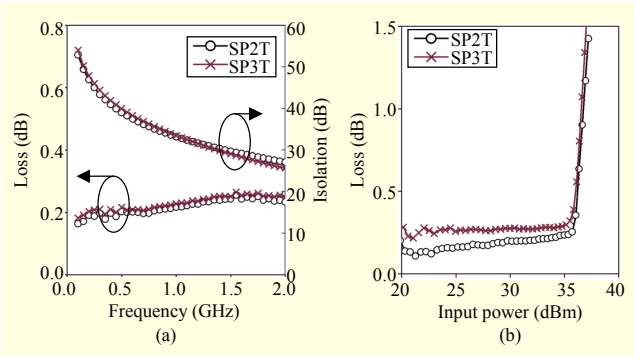

Fig. 11. Measured results of post-PA switches: (a) loss (MAG) and isolation, (b) power endurance.

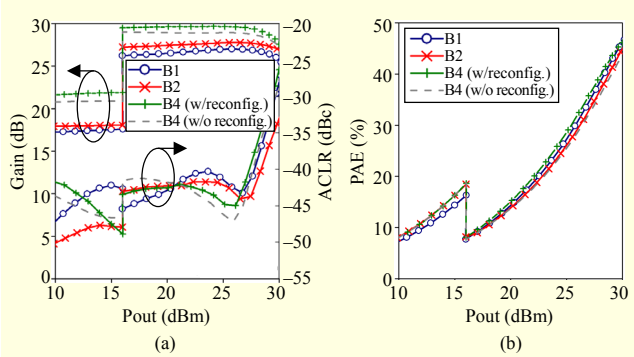

Fig. 12. Measured results for high-band PA operation: (a) gain and ACLR, (b) PAE.

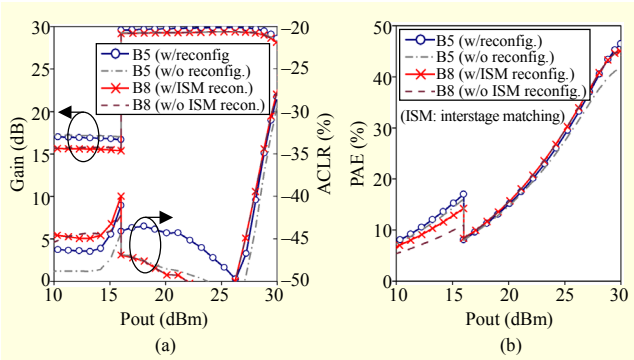

Fig. 13. Measured results for low-band PA operation: (a) gain and ACLR, (b) PAE.

which is large enough to be operated for the UMTS PA output.

The measurement results of power gain, adjacent channel leakage ratio (ACLR), and power-added efficiency (PAE) are shown in Figs. 12 and 13. In the case of the high-band operation shown in Fig. 12, the PA shows power gains of higher than 26.9 dB and ACLRs of better than –39 dBc up to the rated linear output powers (28 dBm at band-1, 28.5 dBm at band-2, and 27.5 dBm at band-4). The PAE at maximum linear power meeting –39 dBc ACLR is higher than 37.5% for all three bands (38% at 28 dBm for band-1, 39% at 28.5 dBm for band-2, and 37.5% at 27.5 dBm for band-4). It should be noted that the band-4 result with power and frequency reconfiguration (M_1 is on) shows better PAE (3.5% improvement) than that without reconfiguration (M_1 is off), while maintaining an ACLR of –39 dBc. In the case of the low-band operation shown in Fig. 13, the PA shows linear power gains of higher than 29.2 dB and ACLRs of better than –39 dBc up to the rated linear output powers of both 28.2 dBm. PAEs at maximum linear power meeting –39 dBc ACLR are higher than 41% for the two bands. It should also be noted that the band-5 result with frequency reconfiguration (M_3 is on) shows better PAE (3% improvement) than that without reconfiguration (M_3 is off), while maintaining a similar ACLR. The measured port-to-port isolation is greater than 28.5 dB for all bands, and no abnormality results from the switch integration.

The idle current is reduced from 100 mA to 20 mA using a stage-bypass approach, and PAEs of higher than 14.3% are measured at 16 dBm. It is noteworthy that the PAE at band-8 with interstage reconfiguration (M_5 is on) shows better PAE (3.3% improvement) than that without reconfiguration.

To validate that most of the nonlinearities are generated from the PA core, as stated in section III, the two-tone third-order intermodulation distortion (IMD3) and the second-/third-harmonic distortion characteristics of the switches and composite PA module (PA + switch) are tested at band-8 as a reference, and the results are plotted in Fig. 14. The IMD3 of the switches (–57 dBc at P_{out} = 28.2 dBm) are nearly the same as that of the signal source, whereas the IMD3 of the composite PA module is –27 dBc at P_{out} = 28.2 dBm. The second harmonic ratios of the switches (–72 dBc at P_{out} = 28.2 dBm) are nearly the same as that of the signal source, whereas the composite second harmonic distortion of the composite PA module is –38 dBc at P_{out} = 28.2 dBm. These results mean that the IMD3 and second-harmonic distortion caused by the switch device can be neglected. Besides, the third-harmonic distortion ratios of the switches are slightly deviated from the signal source (starting from the output power of 27 dBm) but still preserve –69 dBc at P_{out} = 28.2 dBm and are thus far better than that of the composite PA module (–55 dBc at P_{out} = 28.2 dBm). From the results, it can be said that the switch device does not cause any significant effect on nonlinear behavior to the proposed PA module over the entire linear output power region.

The measurement results are summarized in Table 4. For reference, five single-band PAs are also developed using the same die size and stage-bypass technique in this work. Compared with the single-band reference PA using the same PA MMICs and FOMNs, the proposed PA shows PAE

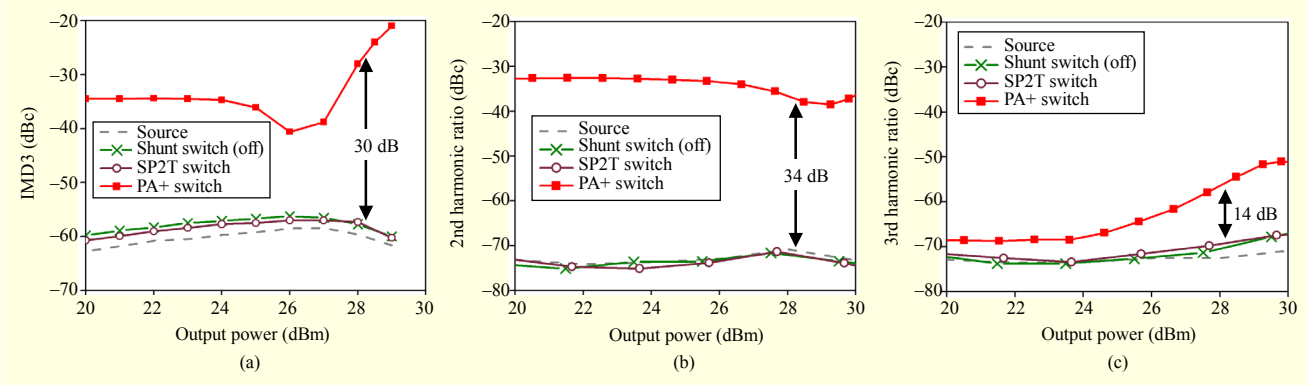

Fig. 14. Measured nonlinear distortions of switches (6-stack) and composite PA module: (a) IMD3, (b) 2nd harmonic ratio, and (c) 3rd harmonic ratio.

Table 4. Summarized results of fabricated reconfigurable PA.

Band	P_{out} (dBm)	PAE (%)	[1)]PAE of single-band PA (%)	[2)]PAE of previous work (%)	ACLR (dBc)	ISO (dB)
B1	28.0	38	41	39	–39.0	28.5
B2	28.5	39	41.9	38.2	–39.0	29.0
B4	27.5	37.5	40.5	36.1	–39.1	31.5
B5	28.2	41	43.5	40.6	–39.1	30.8
B8	28.2	41.1	43.6	40.7	–39.0	35.5

1) PAE of single-band dedicated PA fabricated for reference.

2) PAE of PA [8] assuming that two SP2T post-PA switches with loss of 0.25 dB [15] are additionally used to extend from tri-band to penta-band operation.

Table 5. Performance comparison of reported penta-band UMTS PAs.

References	PA core (switch) technology	P_{out} (dBm), PAE (%)	ACLR (dBc)	Size (mm^2)
Motoyama[1)] 13 [4]	pHEMT (pHEMT)	P_{out} = 28.5 PAE = 40	–38	35
Kim[2)] 12, our previous work [8]	GaAs HBT (PIN diode)	P_{out} = 27.5 - 28.5 PAE = 36.1 - 40.7	–39	32
This work	GaAs HBT (SOI CMOS)	P_{out} = 27.5 - 28.5 PAE = 37.5 - 41.1	–39	25

1) This PA is based on triple stacked-FET structure with separated V_{DD} of each FET, resulting in very large optimum load impedance (R_{opt} = 25 Ω - 30 Ω).

2) Estimated PAE and size assuming that two SP2T post-PA switches [15] are additionally used for penta-band operation.

degradation of 2.5% to 3%, which is attributed to losses from the switches. Also, compared to our previous work [8], assuming that the two SP2T post-PA switches are additionally used to extend the PA to penta-band operation, the PAEs of the proposed PA are improved by OMN optimization, except for the band-1 case. Lower PAE at band-1 of the proposed PA (39% to 38%) is attributed to the quasi-optimum matching at band-1 and higher loss of the switch. It is noteworthy that the PAE improvement of band-4 (36.1% to 37.5%) is much larger than those at the other bands, thanks to the optimum matching of the PFRN proposed in this work, verifying the proposed reconfiguration idea. The performance of recently reported penta-band UMTS PAs is summarized in Table 5. Compared to the PA using pHEMT technology [4], the proposed PA shows smaller module size with comparable linearity and efficiency. Thus, this PA has merits in terms of RF performance and module size by adopting reconfigurable OMN and a fully integrated SOI CMOS switch IC.

V. Conclusion

A fully-integrated 5 mm × 5 mm penta-band (band-1/2/4/5/8) reconfigurable PA was developed for UMTS handset applications. In this work, a new reconfiguration method was proposed for the reconfigured band that requires simultaneous power and frequency back-offs, with fully quantitative analysis to obtain design parameters for the reconfiguration structure requiring simultaneous power and frequency back-offs. For practical use, all switch blocks of the proposed PA were fully integrated using an SOI CMOS process to save on cost and reduce module size. Measured RF characteristics showed linearity better than –39 dBc for all the bands and the efficiency degradation was limited to less than 2.5% to 3% compared to the single-band PA fabricated for reference. No abnormality from the full integration of the switch was observed. With the strong demand for multi-band coverage for global roaming and extending data communication capacity, the proposed PA can be a practical solution for 3G/4G multiband Tx applications.

References

[1] S. Zhang et al., "A Novel Power-Amplifier Module for Quad-

Band Wireless Handset Applications," *IEEE Trans. Microw. Theory Tech.*, vol. 51, no. 11, Nov. 2003, pp. 2203-2210.
[2] H. Jäger et al., "Broadband High-Efficiency Monolithic InGaP/GaAs HBT Power Amplifier for 3G Handset Applications," *IEEE MTT-S Int. Microw. Symp. Dig.*, Seattle, WA, USA, vol. 2, June 2-7, 2002, pp.1035-1038.
[3] "SKY77432 Multi-mode, Multi-band Power Amplifier Module for Next Generation GGE and HSPA Handsets," Skyworks Solutions Inc., Woburn, MA, USA, Feb. 8, 2011.
[4] H. Motoyama et al., "Stacked FET Structure for Multi-band Mobile Terminal Power Amplifier Module," *IEEE MTT-S Int. Microw. Symp. Dig.*, Seattle, WA, USA, June 2-7, 2013, pp. 1-4.
[5] W.C.E. Neo et al., "Adaptive Multi-band Multi-mode Power Amplifier Using Integrated Varactor-Based Tunable Matching Networks," *J. Solid-State Circuits*, vol. 41, no. 9, Sept. 2006, pp. 2166-2176.
[6] A. Fukuda et al., "A 0.9-5-GHz Wide-Range 1W-Class Reconfigurable Power Amplifier Employing RF-MEMS Switches," *IEEE MTT-S Int. Microw. Symp. Dig.*, San Francisco, CA, USA, June 11-16, 2006, pp. 1859-1862.
[7] A. Fukuda et al., "A High Power and Highly Efficient Multi-band Power Amplifier for Mobile Terminals," *IEEE Radio Wireless Symp.*, New Orleans, LA, USA, Jan. 10-14, 2010, pp. 45-48.
[8] U. Kim et al., "A Multiband Reconfigurable Power Amplifier for UMTS Handset Applications," *IEEE Trans. Microw. Theory Tech.*, vol. 60, no. 8, Aug. 2012, pp. 2532-2542.
[9] S. Kang et al., "A Multi-mode Multi-band Reconfigurable Power Amplifier for Low Band GSM/UMTS Handset Applications," *IEEE Topical Conf. PAWR*, Austin, TX, USA, Jan. 20, 2013, pp. 16-18.
[10] H. Xu and K.K. O, "A 31.3-dBm Bulk CMOS T/R Switch Using Stacked Transistors with Sub-design-rule Channel Length in Floated P-wells," *J. Solid-State Circuits*, vol. 42, no. 11, Nov. 2007, pp. 2528-2534.
[11] A.A. Kidwai et al., "(Invited) An Ultra-Low Insertion Loss T/R Switch Fully Integrated with 802.11b/g/n Transceiver in 90 nm CMOS," *IEEE RFIC Symp.*, Atlanta, GA, USA, June 17, 2008, pp. 313-316.
[12] A. Tombak et al., "Cellular Antenna Switches for Multimode Applications Based on a Silicon-on-Insulator Technology," *IEEE RFIC Symp.*, Anaheim, CA, USA, May 23-25, 2010, pp. 271-274.
[13] D. Wang et al., "High Performance SOI RF Switches for Wireless Applications," *IEEE Int. Solid-State and IC Tech. Dig.*, Nov. 2010, pp. 611-614.
[14] J. Kim et al., *High Efficiency Power Amplifier with Multiple Power Modes*, US Patent 6,900,692, issued May 31, 2005.
[15] "MASWSS0204 GaAs SPDT 2.7 V High Power Switch," M/A-COM Technology Solution Inc., Lowell, MA, USA, 2010.

Unha Kim was born in Ulsan, Rep. of Korea, in 1981. He received his BS degree in electrical engineering from Sungkyunkwan University, Suwon, Rep. of Korea, in 2004 and is working toward his PhD degree in electrical engineering at Seoul National University, Seoul, Rep. of Korea. His research interests include multi-mode multi-band (MMMB) reconfigurable PA structure, PA linearization, and load-insensitive PA technique using GaAs and Si devices for mobile applications.

Sungyoon Kang was born in Seoul, Rep. of Korea, in 1983. He received his BS degree in electrical engineering from Hanyang University, Ansan, Rep. of Korea, in 2010 and is currently working toward his PhD degree in electrical engineering at Hanyang University. His current research activities include PA and RFIC design using GaAs and Si devicves for mobile communication systems.

Junghyun Kim was born in Busan, Rep. of Korea. He received his PhD degree in electrical engineering from Seoul National University, Seoul, Rep. of Korea, in 2005. From 2000 to 2007, he was with WavICs, which is now fully owned by Avago Technologies, as an IC designer and a group manager of the IC design group, where he invented the switchless stage-bypass power amplifier architecture called "CoolPAM™." In 2007, he joined the faculty of the Department of Electronic System Engineering, Hanyang University, Rep. of Korea, where he is currently an associate professor. He holds more than 40 patents on power amplifier technology and RFICs. His current research activities include the design of MMICs for mobile communication and millimeter-wave systems, intermodulation analysis, and nonlinear noise analysis of MMICs.

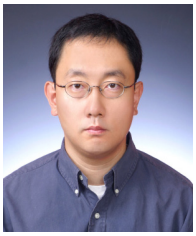

Youngwoo Kwon was born in Seoul, Rep. of Korea, in 1965. He received his BS degree in electronics engineering from Seoul National University, Seoul, Rep. of Korea, in 1988 and his MS and PhD degrees in electrical engineering from the University of Michigan at Ann Arbor, MI, USA, in 1990 and 1994, respectively. From 1994 to 1996, he was with Rockwell Science Center, as a member of the technical staff, where he was involved in the development of millimeter-wave monolithic ICs. In 1996, he joined the faculty of the School of Electrical Engineering, Seoul National University, Seoul, Rep of Korea, where he is currently a professor. He is a co-inventor of the switchless stage-bypass power amplifier architecture called CoolPAM and co-founded Wavics, a power

amplifier design company, which is now fully owned by Avago Technologies. He has authored or co-authored over 150 technical papers appearing in internationally renowned journals and conferences. He holds over 20 patents on RF MEMS and power amplifier technology. Dr. Kwon has been an associate editor for the IEEE Transactions on Microwave Theory and Techniques. He has also served as a technical program committee member of various microwave and semiconductor conferences, including the Microwave Theory and Techniques Society, the RF Integrated Circuit Symposium, and the International Electron Devices Meeting. Over the years, he has directed a number of RF research projects funded by the Korean government and US companies. In 1999, he was awarded a Creative Research Initiative Program by the Korean Ministry of Science and Technology with a nine-year term to develop new technologies in the interdisciplinary area of millimeter-wave electronics, MEMS, and biotechnology. He was the recipient of the Presidential Young Investigator award from the Korean government in 2006.